This article has been accepted and published on J-STAGE in advance of copyediting. Content is final as presented.

IEICE Electronics Express, Vol.xx, No.xx, xx-xx

LETTER

A UWB bandpass filter based on elliptical open stub-loaded resonator and dumbbell-sided cross-circle DGS

Zuxue Xia[1], Rui Wang [1, a)], Wenhai Xia[2], Xin Cao[1] and Xin Xiong[1]

Abstract An Ultra-wideband (UWB) bandpass filter (BPF) based on an elliptical open stub-loaded resonator (EOSLR) and dumbbell-sided cross-circle (DSCC) defected ground structure (DGS) is proposed in this paper. The measured results show that the 3 dB bandwidth of the filter is 3.49 ~ 11.04 GHz, the skirt factor (S.F) is 0.844, the upper stopband rejection is greater than 20 d B at 11.70 ~ 26.80 GHz, and the stopband width is 15.1 GHz. The proposed filter has the advantages of high selectivity and extremely broad upper stopband and it can be applied in UWB Wireless communication system.

key words: UWB, BPF, EOSLR, DSCC DGS
Classification: Microwave and millimeter wave devices, circuits, and hardware

1. Introduction

Since Federal communication commission (FCC) released the band range for UWB (3.1-10.6 GHz) in 2002 [1, 2], UWB filters [3] have attracted significant interest from many scientists and engineers.

There are many technologies for designing UWB BPF, such as the combination of high-pass filter (HPF) and low-pass filter (LPF) [4]; Loading short-circuit stubs technology [5]; Microstrip coplanar waveguide (CPW) technology [6, 7, 8, 9, 10]; substrate integrated waveguide (SIW) technology [11, 12, 13, 14, 15, 16, 17] and Microstrip multimode resonator (MMR) technology [18, 19, 20, 21, 22, 23, 24, 25, 26, 27, 28], et al. Among them, the technology of using microstrip MMR is the most convenient and widely used in recent years. However, MMR-based technology has a narrow upper stopband performance due to spurious harmonics above the desired frequency range. Therefore, the out-of-band resonance characteristics need to be controlled by additional techniques.

In [4, 5], the combination of HPF filter and LPF can suppress the out-of-band harmonics, but the disadvantage is that the size is too large. To improve the stopband performance, Reference [12] proposed a wideband SIW filter based on sawtooth topology, but the occupied area of the structure is obviously large. In [16], the transmission zero (TZ) is introduced through the hybrid coupling structure of rectangular half-mode SIW (RHMSIW), and the upper stopband can reach 20 GHz. In [18], an electromagnetic band gap (EBG) embedded MMR is proposed, which suppresses the fifth resonant mode through EBG, but the stopband was only up to 20 GHz. In [19], by adjusting cross-shaped coupled lines (CCLs) to suppress excess passband, UWB BPF is composed of CCLs and MMR, but the stopband can only reach about 23 GHz. In [27], UWB BPF is simply constructed using only a single-stage parallel coupled line and two rectangular stub resonators, and a tunable TZ is generated by controlling the impedance ratio (R) to extend the wide stopband. At present, the design of UWB BPF mostly adopts uniform impedance resonator (UIR) and stepped impedance resonator (SIR) to design MMR, and a few adopt fan resonator. Elliptical microstrip resonators are mainly used in the design of multi-band filters.

Traditional MMR are composed of rectangular resonators with different impedances or electrical lengths. However, there can be impedance discontinuities where the resonators are connected, resulting in higher parasitic effects, which can increase insertion losses (IL) and reduce bandwidth. In this paper, the rectangular resonator with larger size in MMR is replaced by elliptical resonators, which serve as a transition in impedance variation. And a novel UWB filter based on EOSLR and the DSCC DGSs is proposed. The EOSLR can generate five resonance points at 3~14 GHz, while the elliptical open-circuited stub inside the EOSLR generates a TZ at 3.2 GHz. To facilitate calculation, the odd-even mode resonant frequencies of EOSLR are analyzed theoretically by equating the elliptical resonator to UIR. And DSCC DGSs at the bottom suppress the higher harmonics within 14~25 GHz, extend the upper stopband width, and generate a TZ at 12.7 GHz. The two TZs are located on both sides of the passband, which improves the frequency selectivity. The S.F of proposed

[1]School of Information Engineering, Southwest University of Science and Technology, Mianyang 621000, The People's Republic of China
[2]Zhejiang Lierda Internet of Things Technology Co, Ltd, Hangzhou 311100, The People's Republic of China
[a)] ruiwang@mails.swust.edu.cn

DOI: 10.1587/elex.20.20230159
Received April 06, 2023
Accepted April 24, 2023
Publicized May 09, 2023

Copyright © 2023 The Institute of Electronics, Information and Communication Engineers

design is 0.844, and the upper stopband with a rejection of more than 20 dB is 11.70 GHz to 26.80 GHz.

2. Analysis on the proposed MMR

In this paper, a novel MMR named EOSLR is proposed, and its structure is shown in Fig. 1. EOSLR is composed of symmetrical cascaded two UIRs on the left and right sides of the elliptical resonator, and the elliptical open-circuited stub is loaded at the center.

In order to better analysis, the elliptical resonator can be equivalent to UIR for analysis, which is also a common method to analyze elliptical resonators. The equivalent rectangular MMR is shown in Fig. 2.

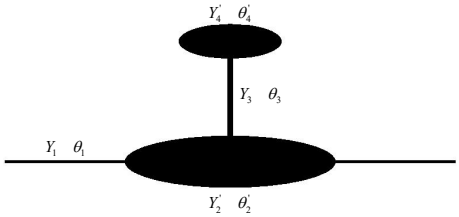


Fig. 1 EOSLR.

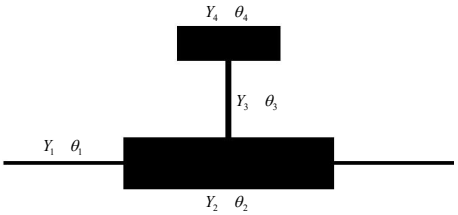


Fig.2 Equivalent rectangular MMR.

The symmetrical MMR can be analyzed by the odd-even mode analysis method. The odd-mode equivalent circuit of the equivalent rectangular resonator is shown in Fig. 3. Under odd-mode excitation, the plane of symmetry is equivalent to a short circuit.

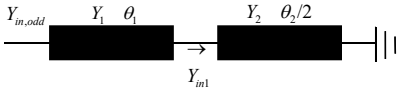


Fig.3 Odd-mode equivalent circuit

$Y_{in,odd}$ is input admittance under odd-mode excitation, odd-mode admittance can be expressed as:

$$Y_{in,odd} = \frac{jY_1 \sin\theta_1 + Y_{in1}\cos\theta_1}{\cos\theta_1 + j\frac{1}{Y_1}Y_{in1}\sin\theta_1} = Y_1\frac{Y_{in1} + jY_1\tan\theta_1}{Y_1 + jY_{in1}\tan\theta_1} \quad (1)$$

$$Y_{in1} = \frac{Y_2}{j\tan\theta_2/2} \quad (2)$$

After bringing Eq. (2) into Eq. (1) we get

$$Y_{in,odd} = Y_1\frac{Y_2 - Y_1\tan\theta_1\tan\theta_2/2}{jY_2\tan\theta_2/2 + jY_2\tan\theta_2/2} \quad (3)$$

According to the theory of microstrip line, if $Y_{in,odd}$ = 0, the odd-mode resonance condition can be obtained.

$$Y_2 - Y_1\tan\theta_1\tan\theta_2/2 = 0 \quad (4)$$

The even-mode equivalent circuit of the equivalent rectangular resonator is shown in Fig. 4.

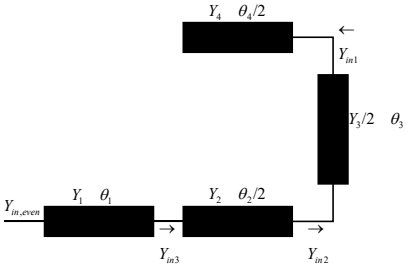


Fig.4 Even-mode equivalent circuit.

Under even-mode excitation, the plane of symmetry is equivalent to an open circuit. $Y_{in,even}$ is input admittance under even-mode excitation, which can be expressed as:

$$Y_{in,even} = \frac{jY_1\sin\theta_1 + Y_{in3}\cos\theta_1}{\cos\theta_1 + j\frac{1}{Y_1}\sin\theta_1} = Y_1\frac{Y_{in3} + jY_1\tan\theta_1}{Y_1 + jY_{in3}\tan\theta_1} \quad (5)$$

$$Y_{in3} = \frac{jY_2\sin\theta_2/2 + Y_{in2}\cos\theta_2/2}{\cos\theta_2/2 + j\frac{1}{Y_2}Y_{in2}\sin\theta_2/2} = Y_2\frac{Y_{in2} + jY_2\tan\theta_2/2}{Y_2 + jY_{in2}\tan\theta_2/2} \quad (6)$$

$$Y_{in2} = \frac{jY_3/2\sin\theta_3 + Y_{in1}\cos\theta_3}{\cos\theta_3 + j\frac{2}{Y_2}Y_{in1}\sin\theta_3} = Y_3\frac{Y_{in1} + jY_3/2\tan\theta_3}{Y_3 + 2jY_{in1}\tan\theta_3} \quad (7)$$

$$Y_{in1} = jY_4\tan\theta_4/2 \quad (8)$$

According to the theory of microstrip line, if $Y_{in,even}$ =0, the odd-mode resonance condition can be obtained.

$$\begin{aligned} &Y_1Y_2Y_3\tan\theta_1 + Y_2^2Y_3\tan\frac{\theta_2}{2} + Y_2\frac{Y_3^2}{2}\tan\theta_3 + Y_2Y_3Y_4\tan\frac{\theta_4}{2} \\ &- Y_1\frac{Y_3^2}{2}\tan\theta_1\tan\frac{\theta_2}{2}\tan\theta_3 - Y_1Y_3Y_4\tan\theta_1\tan\frac{\theta_2}{2}\tan\frac{\theta_4}{2} \\ &- Y_1Y_2Y_4\tan\theta_1\tan\theta_3\tan\frac{\theta_4}{2} - 2Y_2^2Y_4\tan\frac{\theta_2}{2}\tan\theta_3\tan\frac{\theta_4}{2} = 0 \end{aligned} \quad (9)$$

The frequency response of the EOSLR at weak coupling is shown in Fig. 5. The EOSLR has five resonant modes from 3 GHz to 14 GHz. The two resonant frequencies of f_{o1} and f_{o2} are generated by odd-mode, and the three resonant frequencies of f_{e1}, f_{e2} and f_{e3} are generated by even-mode.

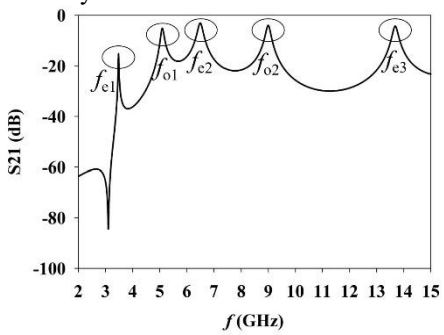
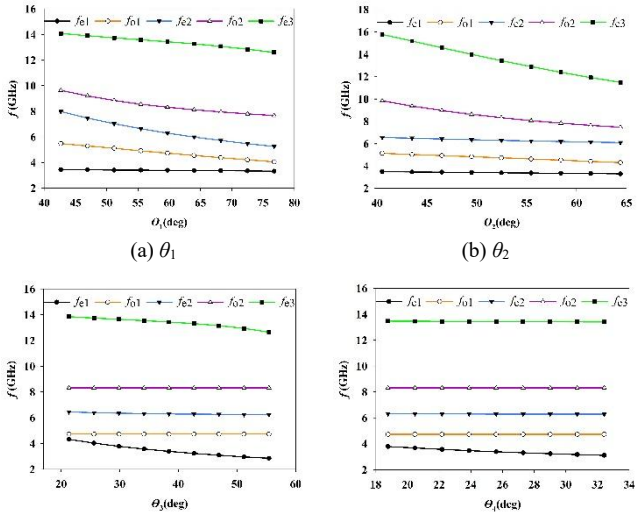


Fig. 5 Resonant frequency response at weak coupling.

Through simulation analysis, the influence of each size parameter on the five resonant frequencies is obtained, and the simulation results are shown in Fig. 6.



(a) θ_1 (b) θ_2

(c) θ_3 (d) θ_4

Fig. 6 The effect of each electrical length in a multimode resonator on its resonant frequency.

In Fig. 6(a), the five resonant frequencies f_{e1}, f_{o1}, f_{e2}, f_{o2} and f_{e3} all decrease with the increase of θ_1. The frequencies of the last four resonant points f_{o1}, f_{e2}, f_{o2} and f_{e3} change greatly, while θ_1 has little influence on f_{e1}. In Fig. 6(b), when θ_2 changes, the five resonant frequencies f_{e1}, f_{o1}, f_{e2}, f_{o2} and f_{e3} all decrease with the increase of θ_2. The frequencies of f_{o1}, f_{o2} and f_{e3} change greatly, while θ_2 has little influence on f_{e1} and f_{e2}. In Fig. 6(c), when θ_3 changes, the resonant frequencies f_{o1} and f_{o2} of the two odd-modes do not change, while f_{e1}, f_{e2} and f_{e3} gradually decrease with the increase of θ_3, and f_{e2} changes slightly. In Fig. 6(d), with the increase of θ_4, the even-mode resonant frequencies f_{e1}, f_{e2} and f_{e3} all decrease, and the changes in f_{e2} and f_{e3} are small, which is difficult to see the obvious change directly, while f_{o1} and f_{o2} remain unchanged. According to previous odd-even mode analysis, the equivalent circuit under odd-mode excitation only exists θ_1 and θ_2. Therefore, the odd-mode resonant frequency is only determined by θ_1 and θ_2, θ_3 and θ_4 does not affect the odd-mode resonant frequency.

When $\theta_2 = 0.976\theta_2^{'}$, $Y_2 = 0.974Y_2^{'}$, $\theta_4 = 0.95\theta_4^{'}$ and $Y_4 = 0.912Y_4^{'}$, the resonant frequencies of the EOSLR are approximately that of the equivalent rectangular MMR, and the results of both are shown in Table I.

Table I. Resonant frequency statistics of EOSLR and equivalent rectangular MMR.

	f_{e1} (GHz)	f_{o1} (GHz)	f_{e2} (GHz)	f_{o2} (GHz)	f_{e3} (GHz)
EOSLR	3.48	5.1	6.51	9	13.69
Equivalent Rectangular Resonator	3.49	4.76	6.34	8.47	13.67

3. Filter design and experimental verification

The three-dimensional view and planar structure of the UWB filter are shown in Fig. 7 and Fig. 8. The filter includes coupled feed ports and EOSLR in the top metal layer, intermediate dielectric layer and DGSs in the bottom metal layer.

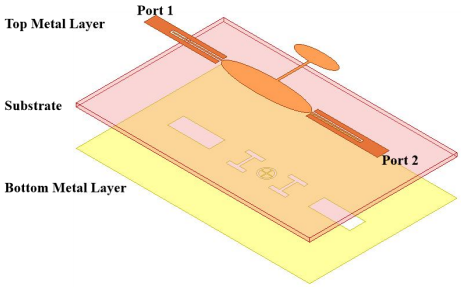
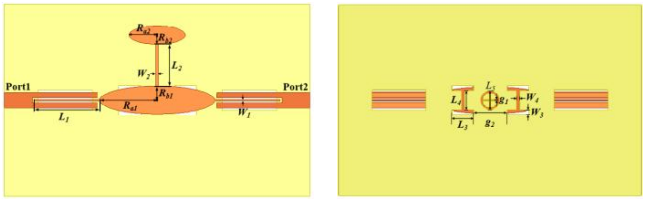


Fig.7 UWB filter three-dimensional structure diagram.



(a) Top layer (b) Bottom layer

Fig.8 Configuration of the proposed UWB BPF.

The two rectangular DGSs at the bottom of the coupling feeder, which is used to form an UWB passband for strong coupling of the filter. And the DSCC DGS in the middle of the bottom consists of two dumbbell-shaped DGS and a cross-circle DGS. Its function is to suppress higher harmonics and generate a TZ on the right side of the passband.

Fig. 9 shows the results of the weak coupling S21 comparison with and without the DSCC DGS. After adding DSCC DGS, higher harmonics in the range of 15 GHz to 25 GHz are significantly suppressed, because DGS acts as a parallel L-C resonator that resonates at specific frequencies based on its size and shape, and can be used for harmonic suppression [29, 30, 31, 32]. Moreover, because the DSCC DGS is located at the bottom of the elliptical resonator in the center of the EOSLR, it changes the equivalent capacitance and inductance of the elliptical resonator. And because the elliptical resonator mainly affects the second, fourth, and fifth resonant frequencies (f_{o1}, f_{o2}, and f_{e3}), after adding the DSCC DGS, the frequencies of f_{o1}, f_{o2}, and f_{e3}

decrease. The results under strong coupling are also compared in Fig. 10. After adding DSCC DGS, the parasitic passband is effectively suppressed, and a transmission zero point is generated at around 12.5 GHz. It can be seen that the stopband bandwidth can extend from 12 GHz to around 25 GHz with a rejection level better than 20 dB.

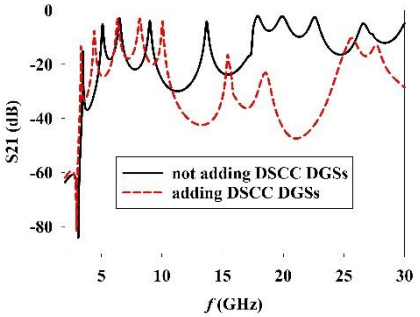


Fig.9 Effect of adding or not adding DSCC DGSs on weak coupling.

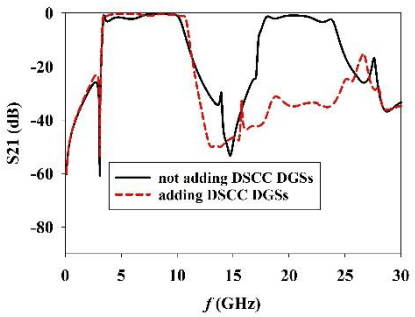


Fig.10 Effect of adding or not adding DSCC DGSs on the strong coupling.

The elliptical open-circuited stub in EOSLR can also generate a TZ, and it is also the elliptical open-circuited stub that generates the first resonant frequency (f_{e1}) of EOSLR, which effectively improves the bandwidth and S.F of UWB filter. The comparison of whether to load the open-circuited stub under weak and strong coupling are shown in Fig. 11 and Fig. 12, respectively. After loading the elliptical open-circuited stub, an additional resonance point and TZ are introduced at the low frequency. Through the comparison of results under strong coupling, loading open-circuited stub also expands the bandwidth and improves the frequency selectivity.

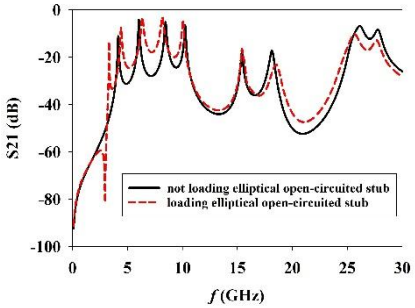


Fig. 11 Effect of whether to load elliptical open-circuited stub on weak coupling.

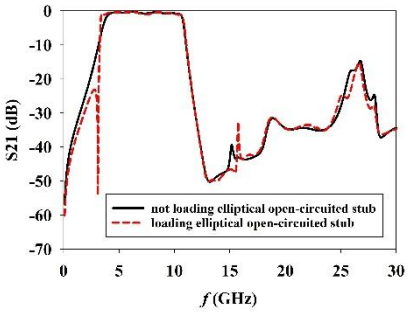


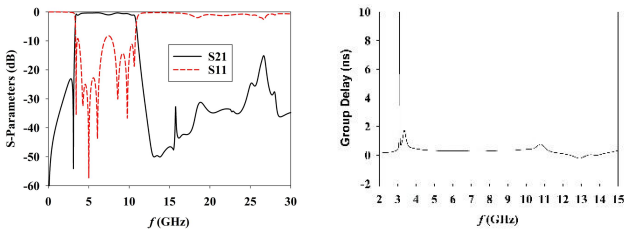
Fig.12 Effect of whether to load elliptical open-circuited stub on weak coupling.

Combined with the above analysis, the specific design parameters of the filter are shown in Table II.

Table Ⅱ. Dimensional parameters of the filter.

Symbol	Value (mm)	Symbol	Value (mm)	Symbol	Value (mm)	Symbol	Value (mm)
W_1	0.15	W_2	0.3	W_3	0.55	W_4	0.35
L_1	7	L_2	4.5	L_3	2.35	L_4	2.1
L_5	2	g_1	0.1	g_2	3.6	R_{a1}	6.15
R_{b1}	1.5	R_{a2}	3	R_{b2}	1		

The simulated S-parameters are shown in Fig.13(a). The simulation result shows that the 3 dB bandwidth range of the filter is 3.33 GHz~10.88 GHz, the relative bandwidth is 106.26%, the insertion loss at the center frequency of 7.1 GHz is -1.14 dB, the return loss is better than - 8 dB, the S.F is 0.858, and the rejection of greater than 20 dB in the upper stopband from 11.45 GHz to 26.14 GHz, and the width is 14.69 GHz. As shown in Fig. 13(b), the group delay in the passband is less than 1.73 ns.



(a) UWB filter simulation S-parameters

(b) UWB filter simulation group time delay

Fig.13 UWB filter simulation results.

Fig. 14 shows the comparison of simulation results of UWB filters based on EOSLR and equivalent rectangular MMR. When the impedance ratio between rectangular resonators in a rectangular MMR is too large, the insertion loss of the filter will significantly increase, while EOSLR using elliptical resonators will improve this disadvantage.

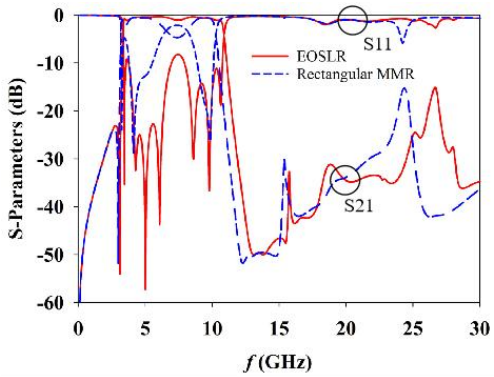
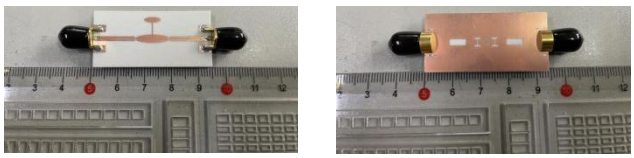


Fig.14 comparison of simulation results of UWB filter based on EOSLR and equivalent rectangular MMR.

Rogers RO4003 (dielectric constant 3.55, thickness 0.508 mm, tangential loss angle 0.0027) is selected as the material for the dielectric substrate in the physical fabrication. Here, the N5247B PNA-X microwave network analyzer of Keysight Technology is used for physical testing. and the photographs of the fabricated filter is shown in Fig.15.



(a) Top layer (b) Bottom layer

Fig.15 Physical picture.

The size of the filter is 26.3×9.6mm^2($1.04\times0.38\lambda_g^2$), and the simulated and measured results are shown in Fig. 16.

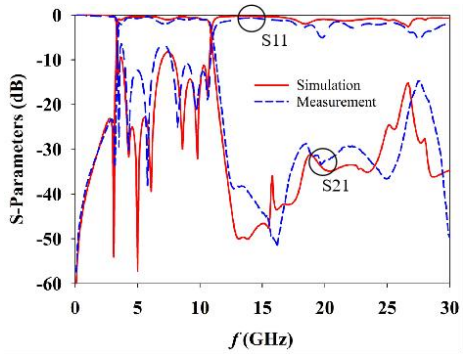


Fig.16 Comparison of simulated and measured UWB filter results.

The measured result shows that the filter has a 3 dB bandwidth range from 3.49 GHz to 11.04 GHz, a relative bandwidth of 103.92 %, an insertion loss of -1.95 dB at the center frequency of 7.1 GHz, a return loss better than -6 dB, and a S.F of 0.844. The upper stopband with rejection greater than 20 dB ranges from 11.70 GHz to 26.80 GHz with a width of 15.1 GHz. The TZs are located at 3.2 GHz and 12.7 GHz, respectively. The measured and simulated results are in good agreement, which proves that the design is feasible, although there is an error between the measured and simulated insertion loss. The error may be that the welding process and the loss and machining accuracy introduced by the SMA connector lead to a larger coupling distance between the feeder and the resonator, which increases the insertion loss.

A comparison between the fabricated UWB BPF and the UWB filters in other similar literature is shown in Table Ⅲ. The designed UWB BPF has the advantages of high selectivity, wide bandwidth and extremely broad upper stopband.

Table III. Comparison of UWB BPFs

Ref.	FBW (%)	S.F.	upper-band rejection
[4]	122	/	20 dB/11.6~20 GHz
[16]	76.3	0.47	20 dB/10.7~14.2 GHz
	89.6	<0.54	20 dB/10.32~13. 9 GHz
	25.2	<0.6	20 dB/10.05~20 GHz
[17]	103.5	<0.7	20 dB/11.4~16.2 GHz
	92.3	0.75	20 dB/9.75~11 GHz
[27]	101.9	/	20 dB/10.9~25.1 GHz
This work	**103.92**	**0.844**	**20 dB/11.70~26.80 GHz**

S.F: selectivity factor of the passband; $\mathrm{S.F}=\frac{\Delta f_{3\mathrm{dB}}}{\Delta f_{30\mathrm{dB}}}$; $\Delta f_{3\mathrm{dB}}$, $\Delta f_{30\mathrm{dB}}$: 3dB bandwidth and 30dB bandwidth of the passband, respectively.

4. Conclusion

In this paper, a UWB BPF with high selectivity and extremely broad upper stopband is proposed, which is composed of EOSLR and DSCC DGSs. Five resonance points in the band from 3 GHz to 14 GHz are generated by EOSLR, and an elliptical open-circuited stub in the EOSLR generates a TZ at 3.2 GHz. Higher harmonics in the band from 14 GHz to 25 GHz are suppressed by DSCC DGSs, which broaden the region of the upper stopband, and DSCC DGSs generate a TZ at 12.7 GHz. The S.F of the measured UWB filter is 0.844, and the upper stopband width is 15.1 GHz. This shown that the UWB filter has the better performance and good engineering value in Microwave communication circuit.

Acknowledgments

This paper was supported by Doctoral Fund Southwest University of Science and Technology (SWUST) (No.19zx7124) and Natural Science Foundation of Sichuan Province (No. 2022NSFSC0953).

References

[1] P. P. Shome, et al.: "Two Decades of UWB Filter Technology: Advances and Emerging Challenges in the Design of UWB Bandpass Filters" IEEE Microwave Magazine **22** (2021) 32 (Doi: 10.1109/MMM.2021.3078040).

[2] H. Yang, et al.: "A Compact Filtering UWB Antenna with band-notched function," IEICE Electronics Express **13** (2018) 20180458 (DOI: 10.1587/elex.15.20180458).

[3] J. Li, "Multi-mode resonators with quad-/penta-/sext-mode resonant characteristics and their applications to bandpass filters," International Journal of RF and Microwave Computer-Aided Engineering **27** (2017) e21072 (DOI: 10.1002/mmce.21072).

[4] R. Ghatak, et al.: "A Compact UWB Bandpass Filter With Embedded SIR as Band Notch Structure." IEEE Microwave & Wireless Components Letters **21** (2011) 261 (DOI: 10.1109/LMWC.2011.2128302)

[5] H. Shaman and J. S. Hong: "Ultra-Wideband （UWB）Bandpass Filter With Embedded Band Notch Structures," IEEE Microwave and Wireless Components Letters **17** (2007) 193 (DOI: 10.1109/LMWC.2006.890467).

[6] X. Lou et al.: "Compact UWB Bandpass Filter With Ultra Narrow Notched Band," IEEE Microwave and Wireless Components Letters **20** (2010) 145 (DOI**:** 10.1109/LMWC.2010.2040212)

[7] J. Gao, et al.: "Short-Circuited CPW Multiple-Mode Resonator for Ultra-Wide-band (UWB) Bandpass Filter," IEEE Microwave and Wireless Components Letters **16** (2006) 104 (DOI: 10.1109/LMWC.2006.869870).

[8] T. -N. Kuo, et al.: "Compact Ultra-Wideband Bandpass Filters Using Composite Microstrip–Coplanar-Waveguide Structure," IEEE Transactions on Microwave Theory and Techniques **54** (2006) 3772 (DOI: 10.1109/TMTT.2006.881624).

[9] L. X, et al.: "An ultra-wideband bandpass filter using hybrid structure of microstrip and CPW," Microwave and Optical Technology Letters **51** (2009) 2257 (DOI: 10.1002/mop.24658)

[10] A. N. Ghazali, et al.: "Dual band notched UWB-BPF based on hybrid microstrip-to-CPW transition," International Journal of Electronics and Communications **86** (2018) 55 (DOI: 10.1016/j.aeue.2018.01.009)

[11] Q. Li and T. Yang: "Compact UWB Half-Mode SIW Bandpass Filter With Fully Reconfigurable Single and Dual Notched Bands," IEEE Transactions on Microwave Theory and Techniques **69** (2021) 65 (DOI: 10.1109/TMTT.2020.3033830).

[12] F. Mira, et al.: "Design of Ultra-Wideband Substrate Integrated Waveguide (SIW) Filters in Zigzag Topology," IEEE Microwave and Wireless Components Letters **19** (2009) 281 (DOI: 10.1109/LMWC.2009.2017589).

[13] J. Liu, et al.: "Miniaturized dual-mode ultra-wideband filter using sector substrate integrated waveguide," Microwave and Optical Technology Letters **63** (2021) 2227 (DOI: 10.1002/mop.32912).

[14] J. Li, et al.: "Compact UWB BPF with notch band based on SW-HMSIW," Electronics Letters **51** (2015) 1298 (DOI: 10.1049/el.2015.0449).

[15] K. Dong, et al.: "Design of a millimeter-wave wideband bandpass filter with novel-slotted substrate integrated waveguide," Microwave and Optical Technology Letters **58** (2016) 2406 (DOI: 10.1002/mop.30060)

[16] L. Huang, et al.: "Compact wideband ridge half-mode substrate integrated waveguide filters," IEEE Transactions on Microwave Theory and Techniques **64** (2016) 3568 (DOI: 10.1109/TMTT.2016.2606385).

[17] L. Huang and S. Zhang: "Ultra-wideband ridged half-mode folded substrate-integrated waveguide filters," IEEE Microwave and Wireless Components Letters **28** (2018) 579 (DOI: 10.1109/LMWC.2018.2835666).

[18] S. W. Wong and L. Zhu: "EBG-Embedded Multiple-Mode Resonator for UWB Bandpass Filter With Improved Upper-Stopband Performance," IEEE Microwave & Wireless Components Letters **17** (2007) 421 (DOI: 10.1109/LMWC.2007.897788).

[19] X. K. Tian, et al.: "A UWB bandpass filter with wide stopband performance using cross-shaped coupled lines," 2012 International Conference on Microwave and Millimeter Wave Technology (ICMMT) **5** (2012) 1 (DOI: 10.1109/ICMMT.2012.6230403).

[20] X Cao, et al.: "An On-Chip Fractally Chipped FBAR Filter With Ba-Zn-Fe-Sc-O Thin Film in 5G-FR2 Millimeter-Wave Band," IEEE Electron Device Letters **44** (2023) 682 (DOI: 10.1109/LED.2023.3250423).

[21] W. Zhu, et al.: "A novel UWB bandpass filter based on compact tri-section SIR," Journal of HeFei University of Technology **35** (2012) 1221 (DOI: 10.3969/j.issn.1003-5060. 2012. 09 .017).

[22] Y. H. He, et al.: "Design of ultra wideband bandpass filter using microstrip three mode resonator," Electronic Measurement Technology **40** (2017) 148 (DOI: 10.19651/j.cnki.emt.2017.05.031).

[23] X. X. Mo and R. Q. Li: "Multimode Resonator-Based Ultra-Wideband Filter Design," Journal of Chengdu University of Information Technology **37** (2022) 144 (DOI: 10.16836/j.cnki.jcuit.2022.02.005).

[24] L Zhu, et al.: "Ultra-wideband (UWB) bandpass filters using multiple-mode resonator," IEEE Microwave and Wireless Components Letters **15** (2005) 796 (DOI: 10.1109/LMWC.2005.859011).

[25] A. Taibi, et al.: "A Novel Design Method for Compact UWB Bandpass Filters," IEEE Microwave and Wireless Components Letters **25** (2015) 4 (DOI: 10.1109/LMWC.2014.2363016).

[26] X. Shi, et al.: "Novel ultra-wideband (UWB) bandpass filter using multiple-mode resonator," IEICE Electronics Express **13** (2016) 20160425 (DOI: 10.1587/elex.13.20160425).

[27] S. -W. Lan, et al.: "Design of a Compact Ultra-Wideband Bandpass Filter With an Extremely Broad Stopband Region," IEEE Microwave and Wireless Components Letters **26** (2016) 392 (DOI: 10.1109/LMWC.2016.2558039).

[28] D. Sarkar, et al.: "An ultra-wideband (UWB) bandpass filter with complementary split ring resonator for coupling improvement," International Journal of Electronics and Communications **71** (2017) 89 (DOI: 10.1016/j.aeue.2016.11.004).

[29] Z. Y. Guo, et al.: "Novel compact ultra-wideband bandpass filter based on vialess vertical CPW/microstrip transitions," Electronics Letters **53** (2017) 1258 (DOI:10.1049/EL.2017.2060).

[30] K. Mohamed, et al.: "A New Class of Highly-Miniaturized Reconfigurable UWB Filters for Multi-Band Multi-Standard Transceiver Architectures," IEEE Access **5** (2017) 1714 (DOI: 10.1109/ACCESS.2017.2670526).

[31] A.T. Jorge, et al.: "A DGS pattern including DMS behavior for compact unit-cell designs," IEICE Electron. Express **16** (2019) 20181010 (DOI: 10.1587/elex.15.20181010).

[32] Z. B. Zeng, et al.: "A common mode filter using DGS-based coupled multiple resonance points for all-pass differential circuit," IEICE Electronics Express **19** (2021) 20210543 (DOI:10.1587/ elex.19.20210543).